Sustainable Recycling of Spent Li-Ion Batteries and Iron Ore Tailings for Cobalt Ferrite Synthesis and Its Dual Applications as a Photocatalyst in Solar Photo-Fenton Process and an Electrochemical Sensor

Jenifer R. Almeida, [*,a] Mayra N. Moura, [a] Luma B. Magnago, [a,b] Ana K. S. Rocha, [a]
Edson L. D. Coelho, [a] Sandra A. D. Ferreira, [a] Maria de Fátima F. Lelis [a] and
Marcos B. J. G. de Freitas [a]

[a]Departamento de Química, Universidade Federal do Espírito Santo, Av. Fernando Ferrari, 514, Goiabeiras,
29075-910 Vitória-ES, Brazil

[b]Instituto Federal de Educação, Ciência e Tecnologia do Espírito Santo, Rodovia BR-259, km 70,
Distrito de Itapina, 29717-000 Colatina-ES, Brazil

This study presents a solution to solid waste problems, focusing on spent lithium-ion batteries (LiBs) and iron ore tailings (IOT) from the Mariana environmental accident in Brazil. The approach involves the production $CoFe_2O_4$ from LiBs and IOT, which serves as a catalyst for solar photo-Fenton reactions for methylene blue (MB) decolorization and as an electrochemical sensor for ascorbic acid (AA) detection. Chemical analysis showed recycling potential, with $45.22 \pm 0.22\%$ m m^{-1} Co from LiBs and $14.9 \pm 1.5\%$ m m^{-1} Fe from IOT, determined by inductively coupled plasma atomic emission spectroscopy (ICP OES) and flame atomic absorption spectrometry (FAAS). The sol-gel synthesized $CoFe_2O_4$ exhibited a crystallite size of 51.9 ± 1.3 nm and agglomerated crystal clusters. Recycled-$CoFe_2O_4$ exhibited a 98.1% MB decolorization efficiency in 60 min under solar irradiation and remained above 92.3% in all 7 reuse cycles. The electrochemical sensor exhibited a coefficient of determination of 0.9987, a sensitivity of 3.352 ± 0.0428 µA mol L^{-1}, and a limit of detection of 0.5511 µM in the concentration range of 1.96 to 23.08 mmol L^{-1} for AA detection. This study demonstrates the potential of recycled-$CoFe_2O_4$ in an environmentally friendly dye removal and as an electrochemical sensor, offering sustainable waste management and resource utilization with solar energy.

Keywords: battery waste, iron ore tailings, cobalt ferrite, dye degradation, solar photo-Fenton, electrochemical sensor

Introduction

Rapid technology advances, increasing consumer demand for electronic products, and shorter product life cycles have made e-waste one of the fastest-growing waste streams in the world. Each year, the global volume of electronic e-waste increases by approximately 4%, yet less than 20% of this total is recycled.[1,2] It is estimated that the global generation of electronic waste (e-waste) will reach 74.7 million metric tons by 2030.[3] Batteries are a particularly concerning source of e-waste, with approximately one billion batteries sold annually in Brazil and Japan, and around 6 billion in the United States and Europe.[4] According to the Brazilian Electronic Waste Report published by Green

Electron[5] in 2023, 65% of the e-waste generated in Brazil comes from mobile phones and smartphones, and 38% from laptops and tablets, with the widespread use of lithium-ion batteries (LiBs) in these devices.

While LiBs are widely used in mobile phones and laptops, the market is currently focused on producing batteries for electric vehicles as part of the transition to less polluting energy sources. As the world strives to reduce carbon emissions, there is an expected increase in demand for energy-efficient solutions to meet the growing demand for electric vehicles and electronic devices is expected to increase, boosting the LiB market by 15% between 2021 and 2026. It is estimated that the number of used LiBs will reach approximately 1.38-6.76 million metric tons by 2035.[6-8] The short lifetime of some lithium-ion applications has led to a high rate of used LiB production. At the end of their useful life, most spent LiBs are disposed of in landfills

or incinerated, significantly increasing environmental liabilities.[3]

At the end of their useful life, LiBs become hazardous solid waste that must be properly disposed of to avoid environmental contamination, as they contain hazardous metals and organic solvents (such as propylene carbonate, ethylene carbonate, dimethyl sulfoxide, polychlorinated dibenzofurans, etc.) in their composition.[9] Improper disposal not only pollutes the environment but also leads to the waste of non-renewable natural resources and valuable metals.[10,11] The primary solution to avoid the problems associated with spent LiBs, such as soil and water contamination, and to reuse these materials as raw materials is through battery recycling.[12-15]

Another environmental and economic challenge is the accumulation of iron ore tailings (IOT), a type of solid waste generated during iron processing with limited reuse potential for reuse by industry. Brazil, the second-largest producer of IOT in the world, produces 290 million of IOT annually, of which 94.58% is stored in dams, 2.87% in tailings piles, and only 0.003% is reused.[16] In 2015, the collapse of the Fundão dam in Mariana, Minas Gerais, Brazil, released over 45 million cubic meters of water and tailings into the environment, resulting in the worst environmental disaster of its kind in the world and the largest in the history of Brazil.[17,18] The disaster resulted in the loss of 19 lives and devastating environmental damage, including the destruction of much of the existing biota and riparian ecosystem.[19] To mitigate further damage, some of the tailings were contained by the Candonga hydroelectric plant and stored in dikes at Fazenda Floresta. Brazilian iron ore typically consists of magnetite (Fe_3O_4) and goethite (α-FeOOH), which contain significant amounts of iron, along with quartz (SiO_2), kaolinite ($Si_2Al_2O_5(OH)_4$), alumina (Al_2O_3), silica (SiO_2), and gibbsite ($Al(OH)_3$).[18,20]

The use of solid waste as a raw material for the production of new materials has been the subject of many environmental protection studies.[21-23] The presence of iron in IOT suggests potential for reuse and recycling in the construction and building materials sector, such as for the synthesis of mortar, concrete, geopolymers, ceramics, and bricks;[24] in technological applications, such as for the synthesis of zeolites, mesoporous silica, carbon nanotubes; in adsorption, battery, and fuel cell applications; and in the production of iron oxide nanoparticles for catalytic applications.[18] IOT has been efficiently used as a catalyst in continuous wastewater treatment processes for the removal of MB dye[25] and in the synthesis of cobalt ferrite for application in the photo/sonocatalytic degradation of Congo Red dye (CR).[26]

Ferrites are magnetic iron compounds with spinel crystal structures and different chemical composition (MFe_2O_4, where M is a divalent metal ion, such as iron (Fe), cobalt (Co), zinc (Zn), nickel (Ni), magnesium (Mg), manganese (Mn), copper (Cu)).[27] These materials have interesting properties, including good catalytic activity, magnetic properties, large surface area, high selectivity, high ionic and electrical conductivity, and high thermal, mechanical, and chemical stability, which are widely studied in various fields.[28]

Recycled ferrites have been the focus of much research, and their multifunctional properties have been exploited for a wide variety of technological purposes,[29] including boron[30] and phosphate removal from wastewater,[31] gas and humidity sensors,[32-34] magnetic resonance imaging,[35] data storage and microwave absorption,[36] oil transport,[37] biomedical applications,[38] capacitors[39] and catalytic reactions.[40-42] The magnetic property of ferrites is highly advantageous in catalytic processes because allows easy, fast, and inexpensive separation of the material from the reaction medium for subsequent reuse.[43-49]

A potential solution to these problems is to combine household waste (e.g., spent LiBs) with industrial waste (e.g., IOT) to synthesize new materials such as cobalt ferrite ($CoFe_2O_4$) and exploit its multiple functionalities, such as photocatalytic and pseudocapacitive properties. $CoFe_2O_4$ has attracted attention due to its multiple advantages, including excellent light stability, broad use of visible light, magnetic recyclability, cost-effectiveness, and corrosion resistance. The flexible positions and valence changes of metal cations within the $CoFe_2O_4$ spinel structure provide abundant active surface sites and enhanced Fenton catalytic activity.[50,51] Several studies have reported the synthesis of $CoFe_2O_4$ and/or LiBs from commercial reagents. Irani *et al.*[52] synthesized $CoFe_2O_4$ and used it in photo-Fenton processes to remove phenol and paracetamol from aqueous solutions. Qiu *et al.*[53] developed cobalt ferrite-graphene oxide composites ($CoFe_2O_4$/RGO) for photo-Fenton reactions targeting methyl orange dye degradation. Moura *et al.*[48] demonstrated efficient heterogeneous photo-Fenton using recycled-$CoFe_2O_4$ from Li-ion batteries as a catalyst for methylene blue (MB) dye decolorization. Vinosha and Das[54] synthesized $CoFe_2O_4$ nanoparticles for photo-Fenton degradation of MB dye. Kalam *et al.*[55] used $CoFe_2O_4$ nanoparticles for MB degradation. $CoFe_2O_4$ has been used as electrochemical sensors for various substances, including guanine,[56] uric acid,[57] bisphenol-A,[58] paracetamol,[59] chitosan,[60] and others. L-Ascorbic acid (AA) is important in biochemical, pharmacological, electrochemical, food processing, and other systems, with its redox properties being particularly attractive.[61,62]

The aim of the study, as an innovation, was to synthesize $CoFe_2O_4$ by recycling two different solid residues: LiBs and IOT. The cathode active material (CAM) of LiBs was used as the cobalt source, while the IOT was used as the iron source. After synthesis, the recycled-$CoFe_2O_4$ was used for application in heterogeneous photo-Fenton reactions for decolorization of MB dye by solar irradiation and applied as a non-enzymatic electrochemical sensor of AA, representing an environmentally friendly and economically advantageous combination of methods. The major contribution of this study is the development of a sustainability promotion strategy to recycle LiBs and IOT from an environmental disaster site, thus giving a second life to these human wastes.

Experimental

Materials

All reagents used in the experiments were of analytical grade. Ultrapure deionized water with resistivity 18.2 MΩ cm⁻¹ (PURELAB Ultra Mk 2, ELGA, High Wycombe, UK) was used at experimental and the required dilutions in the preparation of all samples for further analysis by inductively coupled plasma atomic emission spectroscopy (ICP OES) and flame atomic absorption spectrometry (FAAS). All necessary weighing were performed on an ED224S analytical balance (Sartorius Weighing Technology, Goettingen, Germany) with an accuracy of ± 0.0001 g.

Preparation and characterization of CAM

This study used Samsung® laptop LiBs (7.4 V, 45 Wh, 5950 mAh) manufactured in China in 2012 with a solid polymer electrolyte and pouch cells. Batteries were discharged to eliminate any residual charge. The batteries were then manually disassembled into their main components: casing (metal plastic), polymeric separator, cathode, and anode. The layer containing the CAM was oven-dried (404/D, Nova Ética, São Paulo, Brazil) at 120 °C for 24 h to remove organic solvents.[63] The CAM powder was then lightly scraped off the polymeric current collector and ground with agate mortar and pestle (Metaquímica, Jaraguá do Sul, Brazil) to homogenization and particle size reduce.

A 3.009 g of CAM was leached using 3.0 mol L⁻¹ of HNO_3 (Vetec, Brazil) and 10% (v/v) H_2O_2 (Neon, Brazil) at 80 °C for 2 h under constant stirring using a magnetic stirrer with heating (Nova Ética, São Paulo, Brazil) and then filtered using glass funnel (Laderquímica, Vitória,

Brazil) with quantitative filter paper (Unifil, São Paulo, Brazil).[48] The leached solution was characterized for Al, Co, Cu, Fe, Li, Mn, Ni, and Zn contents by ICP OES in an Optima 7000 DV spectrometer (PerkinElmer, Waltham, USA), using the operating parameters described by Almeida *et al.*,[11] and used in the synthesis.

Preparation and characterization of IOT samples

IOT samples were collected according to the Brazilian standard for solid waste sampling. The collection site was a stacking landfill of dredged tailings pile located at Fazenda Floresta, 3 km from the Risoleta Neves Hydroelectric Power Plant (Candonga Power Plant). Sampling was carried outby the Candonga Project team according to the guidelines of ABNT NBR 10007:2004.[64] IOT samples were declumped and sieved through 2 mm mesh sieves (Bertel, Caieiras, Brazil). The samples were then divided into four subsamples for homogenization and processed to obtain the air-dried fine soil fraction, following the EMBRAPA[65] sample processing procedure for spreading, declumping, drying, sieving, quartering, grinding, and storage. Texture analysis was performed to determine sand, silt, and clay fractions.[66] The air-dried fine soil fraction was ground with an agate mortar and pestle (Metaquímica, Jaraguá do Sul, Brazil) for particle size reduction and used in the experiments without further chemical treatment.

A 12.020 g of the IOT sample was leached with an HCl (Vetec, Rio de Janeiro Brazil) and HNO_3 (Vetec, Rio de Janeiro, Brazil) acid solution in a ratio of 3:1. The leaching process was conducted under constant stirring at 80 ± 5 °C for 2 h using a magnetic stirrer with heating (Nova Ética, São Paulo, Brazil) and then filtered using glass funnel (Laderquímica, Brazil) with quantitative filter paper (Unifil, São Paulo, Brazil). Subsequently, the leached solution was analyzed for Fe content by FAAS using a ZEEnit 700 spectrometer (Analytik Jena, Jena, Germany) and used for the synthesis of recycled-$CoFe_2O_4$.

Recycled-$CoFe_2O_4$ synthesis from CAM and IOT recycled leaching solutions

Recycled-$CoFe_2O_4$ was synthesized from CAM and IOT leach solutions by the sol-gel method. After mixing CAM leachate with IOT leachate, citric acid was added as a complexing agent to promote the formation of the precursor material. The masses of the leached solutions were calculated according to their respective chemical compositions determined by ICP OES and FAAS. The molar ratio of Co/Fe/citric acid molar ratio was

J. Braz. Chem. Soc. **2025**, *36*, 2, e-20240137

3 of 17

1:2:3. Briefly, 50.0 mL of CAM leachate (containing 0.8902 g of Co), 100.0 mL of IOT leachate (containing 1.9497 g of Fe), and 8.8 g of anhydrous citric acid ($C_6H_8O_7$) with 99.89% purity (Neon, Suzano, Brazil) were used. The pH of the final solution was adjusted to 6.0 with NH_4OH (Neon, Suzano, Brazil).[67] The solution was then placed under constant stirring at 85 °C for 2 h using a magnetic stirrer with heating (Nova Ética, São Paulo, Brazil) until the volume decreased and a gel was formed. Then, the gel was oven-dried (404/D, Nova Ética, São Paulo, Brazil) at 110 °C for 12 h to remove the solvents. The precursor material was calcined in a muffle furnace (LF 00212, JUNG, Blumenau, Brazil) at 850 °C for 6 h with a heating rate of 2.3 °C min^{-1}.[68] The calcined material was then ground with an agate mortar and pestle (Metaquímica, Jaraguá do Sul, Brazil), washed with a solution containing 1.0 mol L^{-1} potassium chloride (Synth, Diadema, Brazil), ultrapure water, and 96% (v v^{-1}) ethanol (Quimesp, Guarulhos, Brazil) and oven-dried (404/D, Nova Ética, São Paulo, Brazil) at 80 °C for 24 h.[46] The illustration of the experimental synthesis procedure used in this study is presented in Figure S1 (Supplementary Information (SI) section).

Material characterization

CAM, IOT, and recycled-$CoFe_2O_4$ were characterized by X-ray diffraction (XRD) using a D8 Discover diffractometer (Bruker, Massachusetts, USA) using Cu Kα radiation (λ = 1.54056 nm) at a scan rate of 1° min^{-1} in the 2θ range of 10-90°. The Joint Committee on Powder Diffraction Standards (JCPDS) database was consulted.

Recycled-$CoFe_2O_4$ was characterized by scanning electron microscopy (SEM) and energy dispersive X-ray spectroscopy (EDX), which were performed using a Superscan SSX-550 scanning electron microscope (Shimadzu, Kyoto, Japan) with an accelerating voltage of 25.0 kV and a 4.0 probe. Transmission electron microscopy (TEM) was also conducted using a JEM1400 microscope with 120 kV resolution and a LaB$_6$ filament (JEOL, Tokyo, Japan).

The occurrence of dye adsorption was investigated by analyzing the solutions left in the dark for 60 min before adding the peroxide and starting the photocatalysis.

Fourier transform infrared spectroscopy (FTIR) analyses of recycled-$CoFe_2O_4$ were performed before and after catalysis with MB using a Spectrum 400 spectrometer (PerkinElmer, Waltham, USA), with an attenuated total reflectance (ATR) accessory at a resolution of 2 cm^{-1} and an average of 32 scans.

Photocatalytic study and reusability assessment of recycled-$CoFe_2O_4$ as catalyst in decolorization of MB by solar photo-Fenton

Decolorization of MB with recycled-$CoFe_2O_4$ catalyst (Cat) was carried out according to the experimental conditions: a 50.0 mL solution of 30.0 mg L^{-1} MB (Neon, Suzano, Brazil) at pH 3.0, with additions of 0.03 mol L^{-1} H$_2$O$_2$ and 20.0 mg of catalyst as needed, under solar radiation.

The following systems were prepared and analyzed in triplicate: (*i*) system I: 50.0 mL of MB solution; (*ii*) system II: 50.0 mL of MB solution and 20.0 mg of Cat; (*iii*) system III: 50.0 mL of MB solution and 0.03 mol L^{-1} H$_2$O$_2$; (*iv*) system IV: 50.0 mL of MB solution, 0.03 mol L^{-1} H$_2$O$_2$, and 20.0 mg of Cat.

Meteorological data were collected by the automatic weather station of Vitória, Espírito Santo, Brazil, located approximately 1 km from the municipality. All reaction systems were performed under solar radiation (3050.30 kj m^{-2}).[69]

An aliquot of the solution (without the presence of particles of the recycled-$CoFe_2O_4$ material) from each system was transferred using a disposable Pasteur pipette (Cralplast, Cotia, Brazil) to the quartz cuvette (K22-135Q, Kasvi, São José dos Pinhais, Brazil) followed by UV-Vis analysis. The absorption spectra of the chromophore group of MB were measured at 665 nm using a UV-Vis spectrophotometer (DR 5000, HACH, Iowa, USA) at 0, 15, 30, 45, and 60 min.

An analysis of the solution resulting from the catalysis process by heterogeneous photo-Fenton reaction (system IV) was performed. The contents of the elements Al, Co, Cu, Fe, Li, Mn, Ni, and Zn were determined in the final discolored solution in this system using ICP OES.

For the catalyst reuse study of recycled-$CoFe_2O_4$, after each cycle, the catalyst was separated from the solution using a magnet, washed with distilled water, dried at 60 °C, and reused successively in the photocatalytic reaction similar to system IV.

Electrochemical property of recycled-$CoFe_2O_4$ as a non-enzymatic AA sensor

Preparation of the composite, working electrodes and electrochemical cell

Initially, a composite was prepared by mixing the electroactive material (recycled-$CoFe_2O_4$) and carbon black VXC72 (Boston, USA) in a 90:10 mass ratio. The preparation consisted of dispersing 9.0029 mg of recycled-$CoFe_2O_4$ and 0.996 mg of carbon black in a solution of

400 µL of isopropyl alcohol and 100 µL of Nafion® (Merck, Darmstadt, Germany). This resulted in a solid/liquid ratio of 10 mg 500 µL^{-1}. The mixture was then sonicated at 20 W L^{-1} for 60 min.

The working electrode was prepared using a glassy carbon electrode (GCE) substrate with a geometric area of 0.073 cm^2. The GCE was polished with low-viscosity alumina (eDAQ, ET033, Denistone East, Australia) with a particle size of 0.05 µm, rinsed with distilled water, and dried at 80 °C for 10 min. After polishing and cleaning the electrode, 5 µL of the composite were added to the GCE in two additions of 2.5 µL each, with drying at 80 °C for 10 min after each addition. The electrode was then dried at 80°C for 1 h followed by an additional 24 h at room temperature. The resulting dried composite had a mass of 0.054 mg, and it was referred to as the working electrode modified with recycled-CoFe$_2$O$_4$ (WEM-recycled CoFe$_2$O$_4$).

A conventional three-electrode system was used for the electrochemical studies: the WEM-recycled CoFe$_2$O$_4$ as the working electrode, a platinum wire (0.87 cm^2) as the counter electrode, and an Hg/HgO electrode as the reference electrode. All measurements were performed in a 1.0 mol L^{-1} KOH electrolyte using an Autolab® PGSTAT 302 N potentiostat/galvanostat (Methohm, Herisau, Switzerland).

Cyclic voltammetry (CV) tests were performed using potentiostatic scanning, starting from the open circuit potential with an initial anodic scan up to a potential of 2.0 V, followed by a cathodic scan back to −2.0 V. A scan rate study was performed using values of 100, 75, 50, 25, and 10 mV s^{-1}, each with 5 cycles, to determine the optimal rate for sensor application.

Application of recycled-CoFe$_2$O$_4$ as a non-enzymatic electrochemical sensor for AA

The electrochemical behavior of WEM-recycled CoFe$_2$O$_4$ was evaluated by monitoring the current intensity

as a function of AA concentration. The electrochemical cell was constructed with the WEM-recycled CoFe$_2$O$_4$ as the working electrode, a platinum wire (0.87 cm^2) as the counter electrode, and an Ag/AgCl electrode as the reference electrode immersed in 10 mL of a 0.1 mol L^{-1} phosphate buffer solution (Êxodo Científica, Sumaré, Brazil) at pH 6.6. The voltammetric profile of the sensor was determined by applying stabilization cycles in the potential range of −1.0 to 1.0 V at a scan rate of 100 mV s^{-1} in the anodic direction, starting from 0.0 V in the presence of 0.1 mol L^{-1} phosphate buffer solution. Then, an analytical curve was constructed in a 0.1 mol L^{-1} phosphate buffer solution by measuring the analytical blank and successively adding of 0.1 mol L^{-1} (+)-ascorbic acid (Dinâmica química, Indaiatuba, Brazil) solution. Aliquots of 200 µL were added one by one until reaching the final volume of 3.0 mL, with concentration range of 1.96 to 23.08 mmol L^{-1}. The mixture was stirred for 20 s, and the cyclic voltammogram was recorded after each addition. All electrochemical measurements were performed in triplicate using an Autolab® PGSTAT 302 N potentiostat/galvanostat (Methohm, Herisau, Switzerland).

Results and Discussion

Characterization of recycled materials by XRD, ICP OES, and FAAS

The diffractogram of CAM shown in Figure 1a has characteristic and well-defined peaks of LiCoO$_2$, according to JCPDS 16-427, and a single characteristic peak of graphite carbon, according to JCPDS 8-415, representing a typical CAM composition. The graphitic carbon phase is derived from the additive used to increase the electronic conductivity at the cathode.[11,70]

The diffractogram of IOT shown in Figure 1b has characteristic and well-defined peaks of crystalline hematite (Fe$_2$O$_3$) in a central rhombic phase and quartz (SiO$_2$),
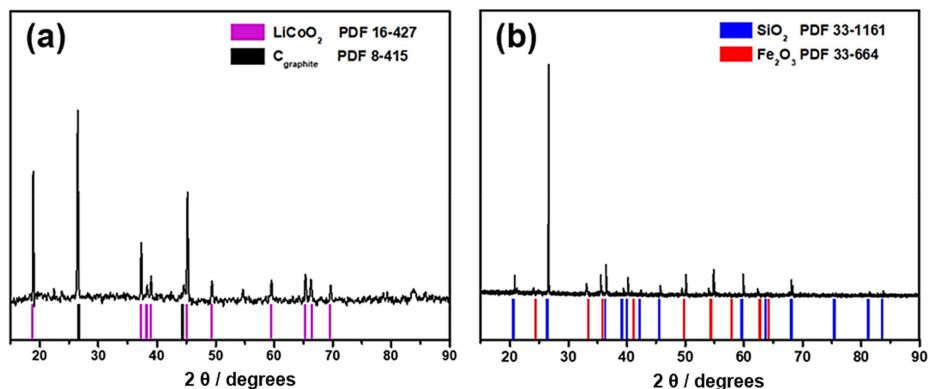
Figure 1. XRD of recycled materials (a) CAM and (b) IOT.

J. Braz. Chem. Soc. **2025**, *36*, 2, e-20240137

5 of 17

according to JCPDS 33-1161 and 33-664, respectively. The weight composition of sand (39.4 ± 0.8% m m^{-1}), silt (49.8 ± 0.7% m m^{-1}), and clay (10.8 ± 0.3% m m^{-1}) fractions was determined by texture analysis. The values were consistent with those of IOT from the Mariana dam disaster in Minas Gerais State, Brazil.[20] Here, tailings were found to be composed of 89% SiO_2 and 11% Fe_2O_3, corroborating the results of Carmignano *et al.*,[18] who reported that IOT typically contains 30-90% SiO_2 and 8-48% Fe_2O_3.

Table 1 shows the results of chemical analysis of CAM by ICP OES and IOT by FAAS. CAM was composed of 45.22 ± 0.22% m m^{-1} Co and 4.91% m m^{-1} Li, as well as traces of Al, Cu, and Fe. The presence of Al and Cu is due to contamination with current collectors. IOT contained 14.9 ± 1.5% m m^{-1} Fe and traces of Al. The chemical composition of the materials indicated a good potential for recycling.

Table 1. Chemical composition of the elements in the samples as a percentage by mass of the recycled materials of cathode active material and iron ore tailing

Element	Cathode active material[a] / (% m m^{-1})	Iron ore tailing[b] / (% m m^{-1})
Al	0.028 ± 0.001	0.275 ± 0.001
Co	45.22 ± 0.22	n.d
Cu	1.08 ± 0.006	n.d
Fe	0.009 ± 0.005	14.9 ± 1.5
Li	4.91 ± 0.07	n.d.
Mn	n.d.	n.d.
Ni	n.d.	n.d.
Zn	n.d.	n.d.

[a]Determined by inductively coupled plasma atomic emission spectroscopy (ICP OES); [b]determined by flame atomic absorption spectrometry (F AAS). n.d.: not detected.

Characterization of recycled-CoFe$_2$O$_4$ by XRD, SEM, EDX and TEM

Figure 2 shows the diffractogram of the recycled-$CoFe_2O_4$, indicating that sufficiently pure $CoFe_2O_4$ has been synthesized. The patterns identified at 2θ values of 18.467, 28.381, 30.358, 35.758, 37.419, 43.460, 53.932, 57.482, 63.140, and 74.684° are attributed to Bragg reflection of the spinel structure (Fd-3m space group, cubic cell), in agreement with JCPDS 1-1121.

The crystallite size (D) of spinel recycled-$CoFe_2O_4$ magnetic nanoparticles was calculated from the average of the most intense peaks using the Debye-Scherrer's equation (equation 1):[71]
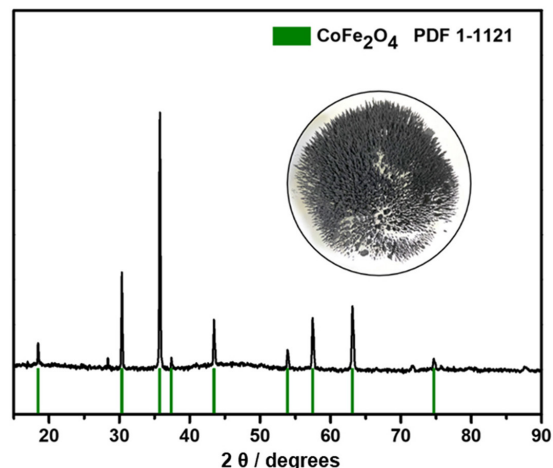
Figure 2. XRD of recycled-CoFe$_2$O$_4$. Inset: magnetic behavior when exposed to a hand magnet.

$$D = \frac{K\,\lambda}{\beta\cos\theta} \tag{1}$$

where D is the size of crystallite size (nm), K is the Scherrer constant, λ is the X-ray wavelength (Cu Kα = 0.154 nm), β is the FWHM (full width at half maximum) of the prominent intense peak (rad), and θ is the Bragg's diffraction angle (rad). Using equation 1, the average crystallite size was 51.9 ± 1.3 nm. The result is consistent with previous studies reporting nanometric particles in the range of 40 to 50 nm.[26] A small average crystallite size indicates a strong synergy between iron and cobalt.[27] Recycled-$CoFe_2O_4$ could be rapidly attracted by an external magnet rapidly (inset of Figure 2), which demonstrated that $CoFe_2O_4$ has magnetic properties. This property of $CoFe_2O_4$ allows for easy separation of the catalyst from the aqueous solution, which favors its reuse in new cycles.

SEM micrographs (Figure 3) were used to examine the morphology of recycled-$CoFe_2O_4$. As shown in Figures 3a and 3b, the material had large agglomerates of crystalline particles grouped into larger conglomerates. The agglomerates were composed mainly of rectangular nanoparticles with an average size of about 50 nm. As discussed by Bessy *et al.*,[72] particle agglomerates, formed to reduce surface energy, are generally the result of magnetic dipole-dipole interactions and van der Waals forces between Fe and Co. The shaded areas in the micrographs in Figures 3c and 3d indicate the presence of voids. A nearly homogeneous distribution of particles was observed, demonstrating the suitability of the sol-gel method for recycled-$CoFe_2O_4$ synthesis.[72]

Figures 4a and 4b show the EDX mapping of recycled-$CoFe_2O_4$ (Figure 4g). The EDX spectrum showed characteristic peaks of Co (Figure 4d), Fe (Figure 4e), and
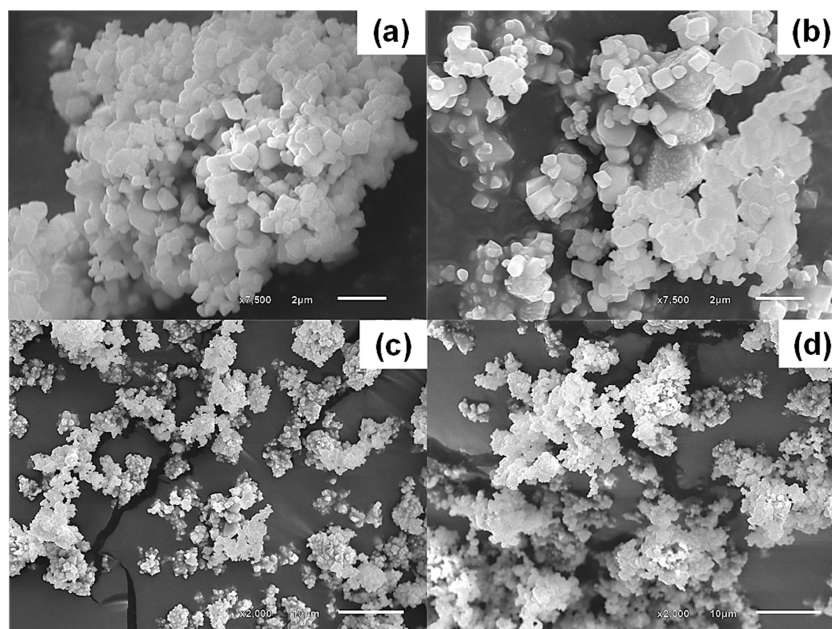
Figure 3. SEM micrographs at different magnifications of recycled-$CoFe_2O_4$: (a, b) 7500×; (c, d) 2000×.

O (Figure 4f), attributed to the spinel phase of synthesized $CoFe_2O_4$. Table 2 shows the weight composition of recycled-$CoFe_2O_4$. The material was found to have a Co/Fe molar ratio of 0.1:0.2, which is consistent with the Co/Fe ratio used. In Figure 4g, the presence of Au and C (Figure 4b) is attributed to the sample coating and Al (Figure 4c) to the sample support.

TEM studies were also performed to evaluate the grain size, morphology, and size distribution. Figure 5 shows the TEM images of recycled-$CoFe_2O_4$, clustering is observed as seen in the SEM analyses. The largest particles reach 200 nm and the smallest are predominantly < 0.25 nm in diameter. These properties are consistent with the face-centered cubic crystal structure of $CoFe_2O_4$, which forms very stable spinel
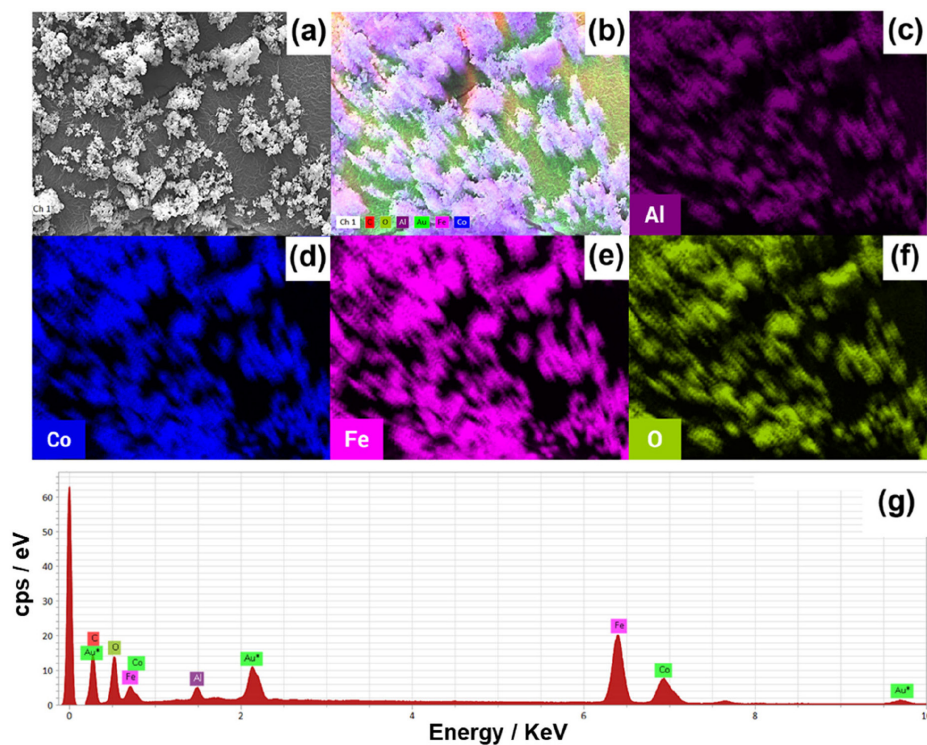
Figure 4. SEM with EDX analysis for recycled-$CoFe_2O_4$ showing the distribution of elements on the surface of the material: (a) micrograph; (b) mapping spectrum; (c) Al mapping (purple); (d) Co mapping (blue); (e) Fe mapping (fuchsia); (f) O mapping (green); and (g) EDX spectrum plot.

J. Braz. Chem. Soc. **2025**, *36*, 2, e-20240137

7 of 17

Table 2. Mass percentage area for the elements in recycled-$CoFe_2O_4$ obtained by energy dispersive X-ray spectroscopy analysis

Element	Mass / (% m m^{-1})
Co	5.65
Fe	13.46
O	66.3

particles, confirming Yang *et al.*,[73] who also recycled Co from LiBs in the sol-gel synthesis of $CoFe_2O_4$. The formation of nanometric scale structures is advantageous because it provides an increase in surface area for possible catalytic applications of the synthesized $CoFe_2O_4$. The nanometric particle size is verified by TEM images and agrees with the results obtained by XRD and Scherrer equation.

Photocatalytic study and reusability assessment of recycled-$CoFe_2O_4$ as catalyst in decolorization of MB by solar photo-Fenton

The decolorization of MB was performed by heterogeneous photo-Fenton with solar radiation and recycled-$CoFe_2O_4$ as catalyst. One of the chromophore groups of MB (Figure S2a, SI section) absorbs radiation at 665 nm, as shown in Figure S2b (SI section). The mechanism of MB degradation is shown in Figure S3

(SI section).[74,75] According to Wen *et al.*,[74] the attack of the hydroxyl radical occurs on the aromatic ring and the bond is broken, generating inorganic ions such as NH_4^+ and NO_3^- and acetic acid.[74] Teng *et al.*[76] stated that homolytic cleavage of the bond occurs of the nitrogen-carbon bond (N–CH$_3$), resulting in the substitution of the methyl group by the hydrogen atom, producing smaller intermediates (HCHO and HCOOH). The C–S and C–N bonds in the central heterocycle of MB are easily broken by free radical attack to produce 2,5-diaminobenzenesulfonic acid and 4-aminocatechol. And then, benzothiazole is generated from 2,5-diaminobenzenesulfonic acid and formaldehyde. Eventually, the aromatic rings break down, producing smaller intermediates that undergo a series of degradation processes to produce CO_2 and H_2O.[76] In previous studies[45,46,48] organic acids environmentally friendly, such as formic acid, acetic acid, and propionic acid were obtained.

Figure 6 shows the MB decolorization was performed by heterogeneous photo-Fenton with solar radiation. A gradual color change of the MB solution was observed with respect to time from blue to light blue and finally twisted to colorless which may be due to decolorization of the chromophore group (Figure 6a). Figures 6b and 6c show the absorption spectra of the MB chromophore group between wavelengths in the range 575-675 nm, with the maximum absorption peak at 665
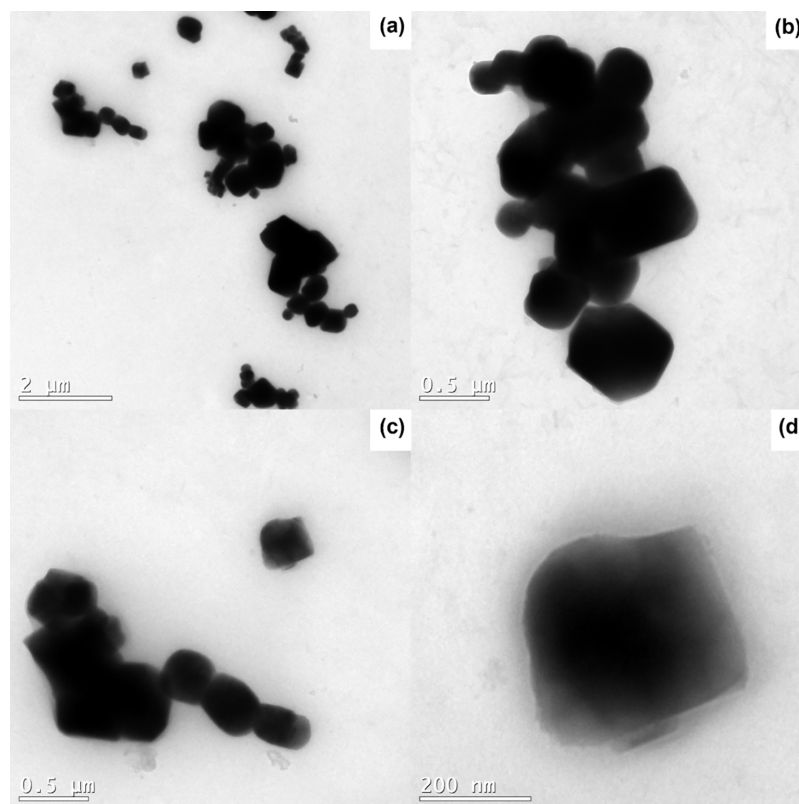
Figure 5. TEM micrographs of recycled-$CoFe_2O_4$ at different magnifications: (a) 2 μm; (b, c) 0.5 μm; (d) 200 nm.

nm. Figure 6b shows the monitoring of the MB dye spectra at times from 0, 15, 30, 45 and 60 min of reaction for systems I, II, III and IV. Figure 6c shows the spectrum of the molecule at the final reaction time of 60 min. The decrease in absorption intensity can be attributed to the π-π* transition of the –N=N– (azo) bond. The peak intensity decreased with time depending on the cleavage of the –N=N– bond, resulting in the disappearance of the blue color of the MB. The decolorization of MB indicates it degradation.[48,77] The decolorization efficiency (D_e) was calculated according to equation 2:

$$D_e = \frac{C_0 - C_t}{C_0} \times 100 \qquad (2)$$

where C_0 is the initial concentration of the MB solution (mg L^{-1}) and C_t is the concentration of the MB solution at time t (mg L^{-1}).

The most likely pathways of MB photocatalytic degradation are outlined in equations 3-8, adapted from Behura *et al.*[26] and Rocha *et al.*[45] Initially, electron/hole pairs (e_{CB}^- / h_{VB}^+) are photogenerated in recycled-$CoFe_2O_4$ under solar irradiation (equation 3). Then, both e_{CB}^- and h_{VB}^+ are involved in the generation of active species such as hydroxyl radicals ($HO^\bullet$) and superoxide radicals ($O_2^{\bullet-}$) (equations 4-7), which react with the dye, leading to its degradation (equation 8).

$$CoFe_2O_4 + h\nu_{solar} \rightarrow CoFe_2O_4 \left(e_{CB}^- + h_{VB}^+\right) \qquad (3)$$
$$e_{CB}^- + (O_2)_{ADS} \rightarrow O_2^{\bullet-} \qquad (4)$$
$$h_{VB}^+ + H_2O \rightarrow H^+ + HO^\bullet \qquad (5)$$
$$O_2^{\bullet-} + H^+ \rightarrow HO_2^\bullet \qquad (6)$$
$$HO_2^\bullet + H_2O \rightarrow H_2O_2 + HO^\bullet \qquad (7)$$
$$HO^\bullet + Dye \rightarrow CO_2 + H_2O + NO_3^- + NH_4^+ + SO_4^{2-} \qquad (8)$$
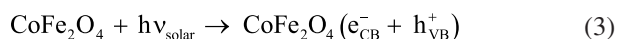
This can be attributed to the formation of the electron-
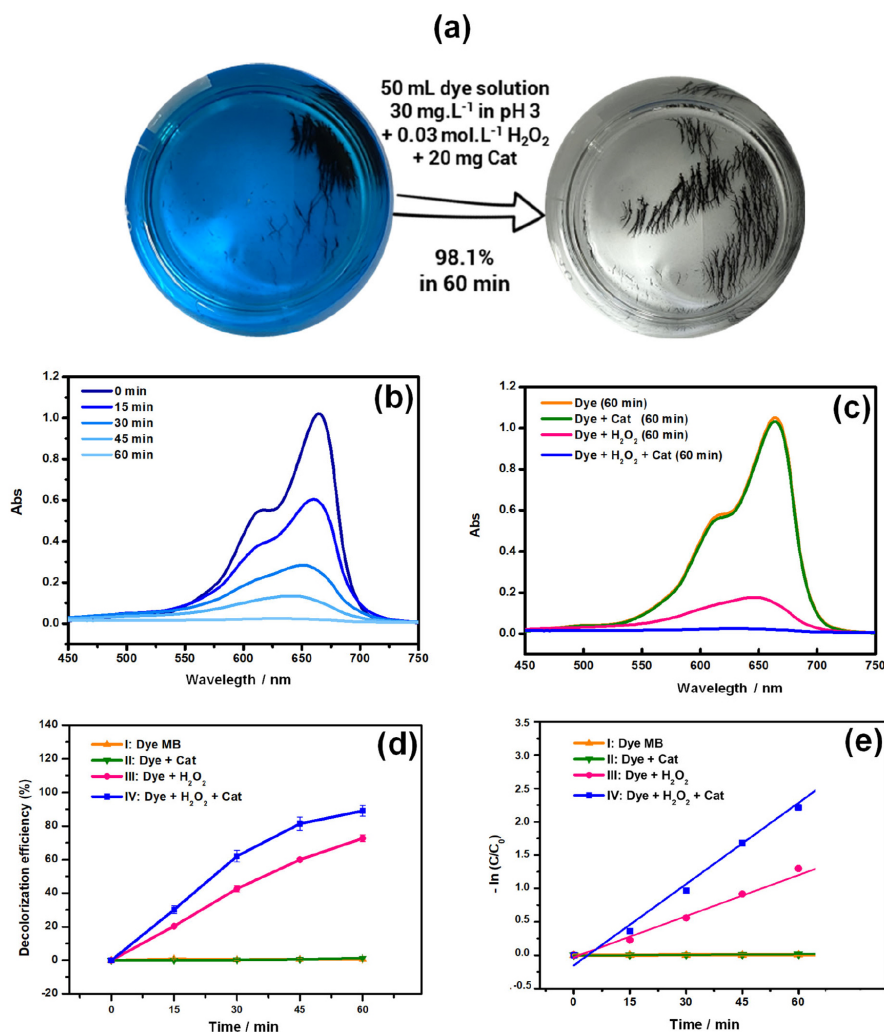
Figure 6. (a) Real representation of the decolorization process under the experimental conditions used; (b) UV spectral sequence of the decrease of the chromophore group at 665 nm at times 0, 15, 30, 45 and 60 min; (c) UV spectral sequence of the decrease of the chromophore group at 665 nm after 60 min; (d) MB decolorization efficiencies at 60 min; (e) first-order kinetic plot (−ln(C/C$_0$) *versus* irradiation time) of MB decolorization.

J. Braz. Chem. Soc. **2025**, *36*, 2, e-20240137

9 of 17

hole pair (e_{CB}^- / h_{VB}^+) on the surface of the magnetic $CoFe_2O_4$ nanoparticles, as mentioned in equation 5, or also to the electrons formed in the reaction mixture, which are directly captured by Fe^{3+} and can react with H_2O_2 to form Fe^{2+}, which in turn can react with H_2O_2 to form hydroxyl radicals, as shown in equation 9.[46]

$$Fe^{2+}_{(surface)} + H_2O_2 \rightarrow Fe^{3+}_{(surface)} + OH^- + HO^\bullet \qquad (9)$$
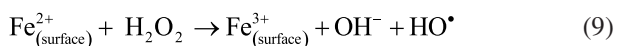
In addition, decolorization can be faster due to high surface area, small size and reduced electron-hole recombination through electronic interaction in magnetic $CoFe_2O_4$ nanoparticles, because materials with small size have high surface area, which provides more surfaces for the dye to adsorb onto the surface would undergo surface reaction with the hydroxyl radical formed on the surface of the catalyst.[55]

The effects of the systems on the decolorization efficiency (%) are shown in Figure 6d. In system I, absorbance measurements were performed to evaluate the effect of solar radiation on MB decolorization. System II was used to evaluate the effect of dye adsorption on the catalyst. System III was used to evaluate the influence of hydrogen peroxide on the photo-Fenton reactions. Finally, system IV was used to evaluate the efficiency of the catalyst in the heterogeneous solar photo-Fenton process. In system I (dye only), solar irradiation was not sufficient to promote decolorization (almost 0%). In system II (dye and catalyst), the effect of adsorption on the decolorization efficiency was insignificant (< 2.6%), furthermore, the use of recycled-$CoFe_2O_4$ as an adsorbent for the MB dye showed no significant efficiency at the studied pH (below 1%), as shown in Figure S4 (SI section). In system III (dye and H_2O_2), the effect of H_2O_2 was significant, resulting in a decolorization efficiency of 76.2% in 60 min. As reported by Casbeer *et al.*,[78] the photo decomposition of H_2O_2 results in the formation of the hydroxyl radical ($HO^\bullet$) (equation 10) where HOO• decomposes rapidly to $HO^\bullet$, a species with higher oxidation potential (E = 2.80 V), exhibiting high reactivity and low selectivity, serving as the primary radical responsible for the dye degradation process Fenton-type.[23,78,79]

$$H_2O_2 + UV \rightarrow 2HO^\bullet \qquad (10)$$

In system IV (dye, catalyst, and H_2O_2), there was a significant increase in decolorization efficiency, reaching 98.1% in 60 min of reaction with the advantage of using solar radiation. The use of solar radiation represents an energy savings, since it eliminates the additional energy expenditure due to the use of artificial radiation, which would require a light booth with UV lamps to simulate solar energy.[23]

The reaction was favored using recycled-$CoFe_2O_4$, was preferred due to its high catalytic oxidation efficiency. The decolorization efficiency was approximately 22% higher in system IV than in system III and 95% higher than in system II. de Freitas *et al.*[25] removed 77% of MB in 240 min of reaction using calcined spherical pellets of recycled IOT. Moura *et al.*[48] achieved 87.7% decolorization efficiency after 420 min of reaction using recycled-$CoFe_2O_4$ from LiB CAM. In the study by Han *et al.*,[80] recycled IOT and green tea were used to synthesize zero valent iron that removed 99.46% of MB in 240 min.

Table 3 shows the comparison of the characteristics of $CoFe_2O_4$ synthesized from different experimental procedures and applied in photocatalysis for dye decolorization. There are few works in the literature on $CoFe_2O_4$ synthesis using recycled reagents. Comparing the result obtained with the other results available in the literature, we have that the $CoFe_2O_4$ synthesized from recycled reagents is as efficient as the $CoFe_2O_4$ synthesized from analytical grade commercial reagents (80-99.75%), and in some cases even more efficient. In this work, the process is more economical and environmentally friendly with green chemistry, since it recycled waste, saved on commercial reagents, used available free energy (solar radiation) dispensing with the use of artificial radiation, and produced an efficient recycled material in the remediation of environmental problems.

Kinetic study of MB decolorization

Figure 6e shows the kinetic study of MB decolorization catalyzed by recycled-$CoFe_2O_4$. A first-order Langmuir-Hinshelwood kinetic model provided the best fit to the experimental data, as shown in equation 11, where C_0 is the initial MB concentration, C is the concentration of the dye at time t, and k is the pseudo first-order rate constant.[26]

$$\ln \frac{C_0}{C} = kt \qquad (11)$$

As shown in the ln (C_0/C) *versus* time plot (Figure 6e), the k values and coefficients of determination (R^2) were 0.00006 L mg^{-1} min^{-1} and 0.75000 for system I, 0.00042 min^{-1} and 0.85026 for system II, 0.02422 min^{-1} and 0.99437 for system III, and 0.06457 min^{-1} and 0.95438 for system IV, respectively.

The half-life ($t_{1/2}$) was calculated using equation 12[46] and was found to be 11550 min for system I, 1650 min for system II, 28.6 min for system III, and 10.7 min for

Table 3. Comparison of the characteristics of synthesized $CoFe_2O_4$ in terms of discoloration efficiency, reaction time, and catalyst crystallite size using commercial and recycled reagent sources through different synthesis methods, with application in photocatalysis for the discoloration of different dyes under various experimental conditions

Iron and cobalt source	Synthesis method	Dye	Experimental decolorization conditions	Radiation source	Decolorization efficiencies and reaction time	Catalyst crystallite size calculate by Debye-Scherrer equation / nm	Reference
Fe from IOT (Mariana, Brazil) and Co from spent LiBs	inorganic acid leaching using HNO_3 and HCl from wastes followed by sol-gel synthesis	methylene blue	pH 3.0 50 mL de dye solution (30 mg L^{-1} of dye) 0.03 mol L^{-1} of H_2O_2 20.0 mg catalyst	solar radiation	98.1% in 60 min	51.9 ± 1.3	this article
Fe from IOT (Odisha, India) and Co from LiBs recycled	inorganic acid leaching using HCl and H_2SO_4 from the tailings, recovery of Co by precipitation with $Na_2S_2O_8$ followed by synthesis by coprecipitation using urea	Congo red	pH ca. 6.3 ± 0.1 100 mL de dye solution (10-40 mg L^{-1} of dye) 0.05-0.2 g catalyst	visible light (high pressure mercury lamp (125 W) and ultrasonic power (20 KHz and 150 W power)	85.6 and 87.4% in 180 min	41.2	26
Fe from analytical grade commercial reagents and Co from spent LiBs	inorganic acid leaching of LiBs using HNO_3 and H_2O_2, followed by coprecipitation synthesis using NH_4OH	methylene blue	pH 3.0 17 mL of dye solution (4.8 mg L^{-1} of dye) 8.0 mL of 3% H_2O_2 (v/v) 30.0 mg catalyst	irradiation in cabin using UV light (20 W)	87.7% in 420 min	18.5	48
Fe and Co from analytical grade commercial reagents	dissolution of $Fe(NO_3)_2 \cdot 6H_2O$ and $Co(NO_3)_2 \cdot 6H_2O$ reagents, followed by synthesis by coprecipitation using NH_4OH	methylene blue	pH 3.0 17 mL of dye solution (4.8 mg L^{-1} of dye) 8.0 mL of 3% H_2O_2 (v/v) 30.0 mg catalyst	irradiation in cabin using UV light (20 W)	87.3% in 420 min	18.4	48
Fe and Co from analytical grade commercial reagents	dissolution of $FeCl_3 \cdot 6H_2O$ and $CoCl_2 \cdot 6H_2O$, followed by synthesis of the modified solvothermal using NaOH	methylene blue	pH not informed 50 mL of dye solution (10 mg L^{-1} of dye) 5.0 mM H_2O_2 0.01 g L^{-1} catalyst	solar light simulator	80% in 140 min	15.0	55
Fe and Co from analytical grade commercial reagents	dissolution of $Fe(NO_3)_2 \cdot 6H_2O$ and $Co(NO_3)_2 \cdot 6H_2O$ reagents, followed by synthesis by chemical precipitation using NaOH	methylene blue	pH 3.0 50 mg L^{-1} of dye solution 25 mM H_2O_2 0.25 g L^{-1} catalyst	near UV radiation using visible light with a high-pressure mercury lamp (165 W)	99.75% in 300 min	5.84	77
Fe and Co from analytical grade commercial reagents	dissolution of $Fe(NO_3)_2 \cdot 6H_2O$ and $Co(NO_3)_2 \cdot 6H_2O$ reagents, followed by hydrothermal synthesis using NaOH	methylene blue	pH 5.0 100 mL dye solution (10 mg L^{-1} of dye) 12 mM of oxidant 10 mg L^{-1} of catalyst	digital chamber equipped with ultraviolet irradiations (18 W)	99% in 60 min	15.4	81

LiBs: lithium-ion batteries; IOT: iron ore tailings.

J. Braz. Chem. Soc. **2025**, *36*, 2, e-20240137

11 of 17

system IV.

$$t_{1/2} = \frac{0.693}{k} \tag{12}$$

The use of recycled-$CoFe_2O_4$ as a catalyst in the presence of H_2O_2 under the conditions specified in system IV provided a fast (60 min, with $t_{1/2} = 10.7$ min) and efficient (98.1%) decolorization of MB, as supported by the rate constant ($k = 0.06457$ min^{-1}) and the coefficient of determination ($R^2 = 0.95438$) of the first-order reaction. The determinant step of the reaction rate was hydroxyl radical formation.[48]

Reuse of recycled-$CoFe_2O_4$

Figure S5 (SI section) presents the reuse performance of the recycled-$CoFe_2O_4$ over seven cycles of MB decolorization. The conditions were the same in all cycles (30.0 mg L^{-1} MB dye, 0.03 mol L^{-1} H_2O_2, 20.0 mg of recycled-$CoFe_2O_4$, pH 3, 60 min, solar irradiation). The decolorization efficiency remained above 92.3% in all 7 reuse cycles. The decolorization efficiency results obtained for each cycle were: 1st cycle: 92.5 ± 0.56%; 2nd cycle: 92.3 ± 0.89%; 3rd cycle: 92.7 ± 0.31%; 4th cycle: 95.6 ± 0.65%; 5th cycle: 97.8 ± 0.42%; 6th cycle: 99.7 ± 0.35%; and 7th cycle: 98.9 ± 0.26%. The maintenance of efficiency across cycles demonstrates that the material exhibits high stability and can be reused and applied practically for textile effluent treatment.

XRD characterization of recycled-$CoFe_2O_4$ before and after catalysis

The XRD analysis of the catalyst material was compared before and after catalysis (Figure S6, SI section). The integrity of the catalyst is verified after the cycles, as there was no change in the XRD profile of the materials, with the presence of the same peaks related to $CoFe_2O_4$ as seen in Figure 2.

FTIR characterization of recycled-$CoFe_2O_4$ before and after catalysis

Figure 7 shows the FTIR spectrum of recycled-$CoFe_2O_4$ before (Figure 7a) and after (Figure 7b) catalysis. Initially, the MB fingerprint region was analyzed, which is located in the region below 1700 cm^{-1}, as can be identified in the FTIR spectrum of the dye (Figure S7, SI section). A prominent band near 1050 cm^{-1} in Figure 7a, before photocatalysis, likely corresponds to the C−O bond of the

primary alcohol, stemming from the washing with ethyl alcohol in the final step of the synthesis procedure. This band remained prominent in the spectrum after catalysis (Figure 7b) and may be associated with the S=O bond of sulfoxides, such as leucomethylene blue sulfoxide, a product formed in the reaction mechanism. Additionally, a minor highlight of the band at 1645 cm^{-1} can be observed in Figure 7b, possibly related to the C=C present in the structure of this product.[82]
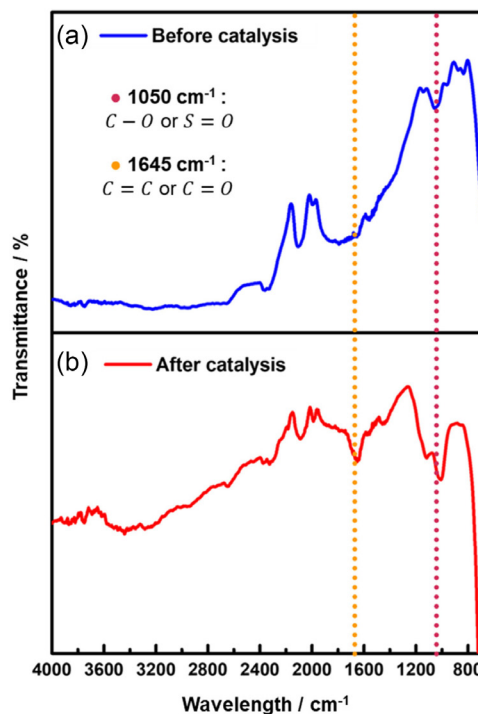
Figure 7. FTIR-ATR spectrum of recycled-$CoFe_2O_4$ (a) before and (b) after catalysis.

Characterization by ICP OES of the MB decolorization solution after solar photo-Fenton process

An evaluation of heterogeneous photo-Fenton catalysis under solar irradiation was performed for system IV. Concentrations of Al, Co, Cu, Fe, Li, Mn, Ni, and Zn were determined by ICP OES in the decolorized final solution. Table 4 shows the element concentrations (mg L^{-1}) along with the maximum allowable values (mg L^{-1}) according to the Brazil's Conselho Nacional do Meio Ambiente (CONAMA) Resolution No. 430/2011 for effluent disposal standards.[83]

For dissolved iron, CONAMA Resolution No. 430/2011 establishes a maximum limit of 15 mg L^{-1}.[83] In this case, the iron content remained below the limit of quantification, ensuring compliance. Other regulated elements, such as Mn, Ni, and Zn, were not detected. As a result, the solution does not pose an environmental risk

Table 4. Concentration of chemical elements in the final catalytic solution after decolorization determined by inductively coupled plasma atomic emission spectroscopy and compared with standard effluent disposal values

Element	Concentration / (mg L^{-1})	Standard values for effluent release according to the CONAMA Resolution No. 430/2011[83]
Al	1.20 ± 0.03	n.a.
Co	0.41 ± 0.05	n.a.
Cu	< LOQ	1.0
Fe	< LOQ	15.0
Li	0.44 ± 0.07	n.a.
Mn	n.d.	1.0
Ni	n.d.	2.0
Zn	n.d.	5.0

LOQ: limit of quantification: LOQ_{Cu} = 0.55 mg L^{-1}; LOQ_{Fe} = 0.07 mg L^{-1}; n.d.: not detected; n.a.: not available in the legislation presented.

when disposed of, in accordance with the principles of Green Chemistry.

Electrochemical property of recycled-CoFe$_2$O$_4$

Figure 8a shows cyclic voltammograms of recycled-CoFe$_2$O$_4$ within a potential range of -2.0 to 2.0 V *vs.* Hg/HgO in KOH aqueous solution 1.0 mol L^{-1}, at scan rates of 100, 75, 50, 25, and 10 mV s^{-1}, starting from -2.0 V *vs.* Hg/HgO in the anodic direction. The observed peak at 1.55 V *vs.* Hg/HgO may be related to the oxidation of Co^{2+} within the ferrite structure to Co^{3+}, forming CoOOH (equation 13). Cathodic peaks are observed at -0.45 V *vs.* Hg/HgO and -0.95 V *vs.* Hg/HgO, possibly related to the reduction of Fe^{3+} to Fe^{2+} and the reduction of Co^{3+} to Co^{2+}.[84]
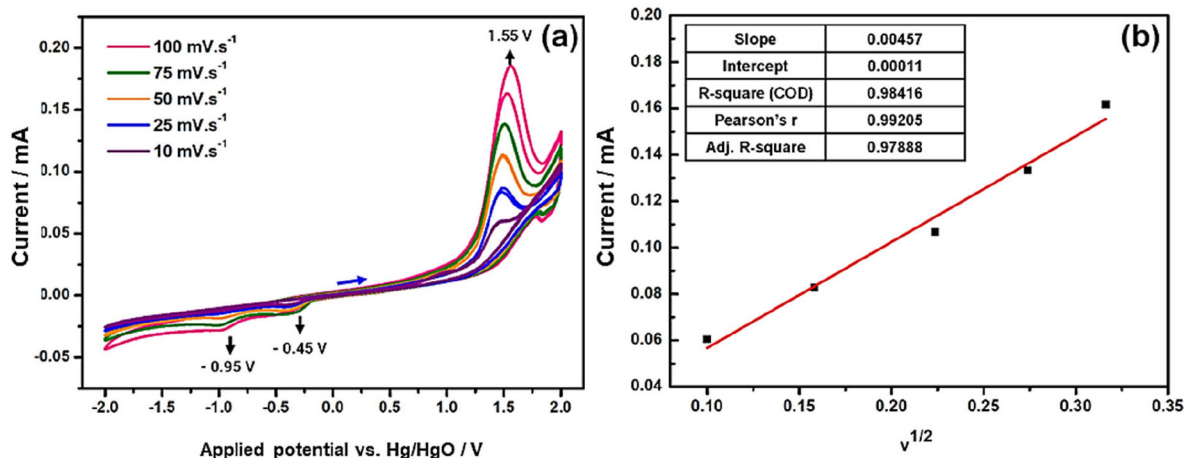
$$CoFe_2O_4 + OH^- + H_2O \rightleftharpoons 2\ FeOOH + CoOOH + e^- \quad (13)$$

The increase observed in anodic peak currents observed with higher scan rates can be attributed to ion diffusion from the electrolyte to the electrode surface. The Randles-Sevcik equation (equation 14) is a mathematical relationship that relates peak currents and scan rate obtained by cyclic voltammetry for an irreversible process at 293 K controlled by diffusion:

$$I_p = (2{,}99 \times 10^5)\, n^{3/2} A\, C D^{1/2}\ v^{1/2} \quad (14)$$

where I_p represents the peak current; n is the total number of electrons transferred; A is the electroactive surface area of the electrode; D is the diffusion coefficient (cm^2 s^{-1}), and v is the scan rate (V s^{-1}). According to equation 14, the peak current is directly proportional to concentration and increases with the square root of the scan rate. By relating the peak currents obtained at the anodic peak potential of 1.55 V to the square root of each employed scan rate, the graph and its corresponding equation were derived, as shown in Figure 8b. The linearity of the graphic, with a coefficient of determination of 0.9842, indicates that the electrode reaction is governed by mass transport, implying the process is diffusion-controlled by electrolyte diffusion towards the electrode/solution interface.

Performance of recycled-CoFe$_2$O$_4$ as a non-enzymatic AA electrochemical sensor

The performance of the electrochemical sensor based on recycled-CoFe$_2$O$_4$ was investigated at different concentrations of AA solution. Figure 9a shows the voltammogram of WEM-recycled CoFe$_2$O$_4$ in the absence (black) and the presence (colored) of AA in the range of 1.96 to 23.08 mmol L^{-1} in 0.1 mol L^{-1} phosphate buffer. An anodic peak close to 0.5 V was observed, which is attributed

Figure 8. (a) Cyclic voltammogram at different sweep rates in the potential range from -2.0 to 2.0 V in 1.0 mol L^{-1} KOH using WEM-recycled CoFe$_2$O$_4$. (b) Graph of peak current *versus* square root of sweep rate for WEM-recycled CoFe$_2$O$_4$.

J. Braz. Chem. Soc. **2025**, *36*, 2, e-20240137

13 of 17

to the oxidation of AA ($C_6H_8O_6$) to dehydroascorbic acid (DHA, $C_6H_6O_6$), as described in equation 15.

$$C_6H_8O_{6\,(aq)} \rightleftharpoons 2C_6H_6O_{6\,(aq)} + 2H^+_{(aq)} + 2e^- \qquad (15)$$
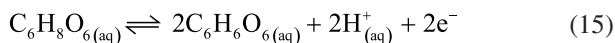
The intensity of the peak increased linearly with AA concentration. Figure 9b shows a good linearity between the peak current and the AA concentration, with an R^2 of 0.9987. The application of recycled-$CoFe_2O_4$ as non-enzymatic electrochemical sensors for the detection of AA is original and presents a few similar works in the literature. Recycled-$CoFe_2O_4$ from LiBs and IOT has an excellent sensitivity (3.352 ± 0.0428 µA mol L^{-1}). The performance of the fabricated electrochemical sensor is thus comparable to other systems that work based on the electrocatalytic oxidation of AA 24.46 µA mol L^{-1},[85] and 49.8 ± 0.0023 µA mol L^{-1} respectively.[10]

The CV analysis of the WEM-recycled $CoFe_2O_4$ blank in 0.1 mol L^{-1} phosphate buffer at pH 6.6 and a scan speed of 100 mV s^{-1} was conducted. This analysis evaluated only the measurement of the WEM-recycled $CoFe_2O_4$ in the presence of the phosphate buffer solution. It was found that in the absence of AA, there was no analytical response from the recycled-$CoFe_2O_4$ that could identify any redox process, as shown in Figure S8 (SI section). Therefore, it is ensured that the electrochemical response observed in the above sections is related to AA.

The main performance characteristics of the technique were estimated from the analytical curve, calculated according to Leal *et al.*,[62] and are described in Table 5. The results confirm the good efficiency of the working electrode modified by recycled-$CoFe_2O_4$ for the determination of AA concentrations. The use of recycled-$CoFe_2O_4$ as an electrochemical sensor represents an innovative and environmentally friendly solution for preserving the

Table 5. Performance characteristics of sensitivity, limit of detection, limit of quantification, range, and coefficient of determination obtained for recycled-$CoFe_2O_4$ as an electrochemical sensor in the determination of AA

Performance characteristics	Value
Sensitivity / (µA mol L^{-1})	3.352 ± 0.0428
Limit of detection / µM	0.5511
Limit of quantification / µM	1.8370
Range / (mmol L^{-1})	1.96 to 23.08
Coefficient of determination (R^2)	0.9987

environmental and reducing the environmental impact of improper waste disposal.

According to the literature,[10,62,86] limits of detection ranged from µM to nM and lower. Electrochemical detection is an attractive alternative for electroactive species, due to its inherent advantages of simplicity, ease of miniaturization, high sensitivity, and relatively low cost. According to Thu *et al.*,[86] the quantification of AA in pharmaceutical formulations and beverage samples can be achieved using the differential pulse anodic stripping voltametric method with a glassy carbon electrode modified with $CoFe_2O_4$. The limits of detection were obtained in the linear range of 0.2-4.4 µM, with 0.313 µM for AA. The concentrations determined by electrochemical detection are comparable to those obtained by high-performance liquid chromatography (HPLC).

Conclusions

This study demonstrated the potential of using CAM from spent LiBs and IOT for the synthesis of nanostructured spinel ferrites of cobalt and iron, respectively. The composition of the starting materials demonstrated their potential for recycling, with LiB
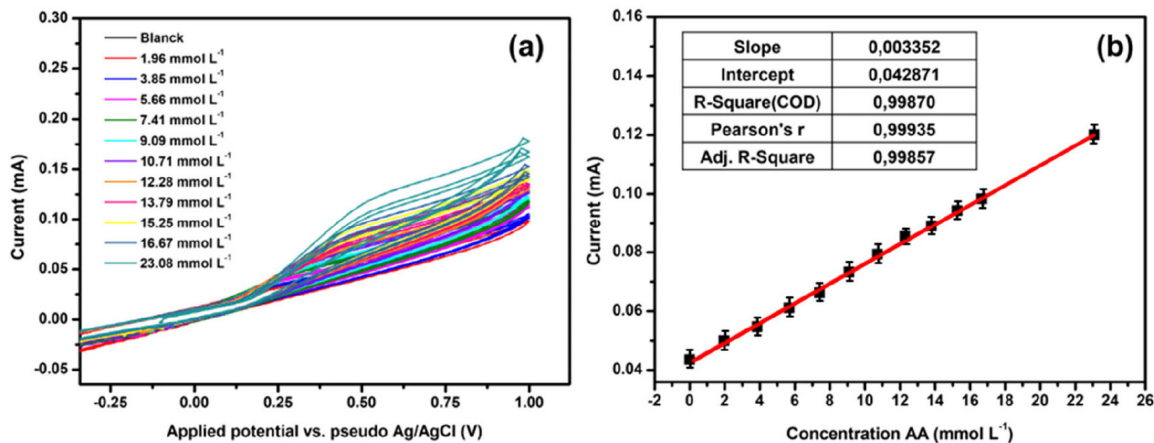
Figure 9. (a) Cyclic voltammograms of WEM-recycled $CoFe_2O_4$ evaluated as an electrochemical sensor in the presence of AA at different concentrations in phosphate buffer 0.1 mol L^{-1} at pH 6.6 and scanning rate 100 mV s^{-1}. (b) Analytical curve relating the anodic peak current to the AA concentration of WEM-recycled $CoFe_2O_4$ evaluated as an electrochemical sensor.

containing $45.22 \pm 0.22\%$ m m^{-1} Co and IOT containing $14.9 \pm 1.5\%$ m m^{-1} Fe. XRD confirmed the formation of the CoFe$_2$O$_4$ spinel structure. The CoFe$_2$O$_4$, synthesized by the sol-gel method, was composed of nanosized particles, and contained $5.65 \pm 0.18\%$ m m^{-1} Co and $13.46 \pm 0.38\%$ m m^{-1} Fe, consistent with the 1:2 ratio of Co/Fe ratio used in ferrite synthesis, as shown by SEM-EDX. Recycled-CoFe$_2$O$_4$ showed magnetic behavior when exposed to a hand magnet, indicating the possibility of magnetic recovery of the material from reaction media, which favors reuse. In a heterogeneous solar photo-Fenton reaction, recycled-CoFe$_2$O$_4$ provided a MB decolorization efficiency of 98.1% in 60 min, and remained above 92.3% across all 7 reuse cycles. This stability indicates the suitability of the material for practical application in textile effluent treatment. The process can be performed outdoors using solar radiation, eliminating the need for artificial radiation. The discolored final solution does not pose an environmental risk when discarded in terms of the inorganic parameters evaluated, in line with the principles of Green Chemistry. The recycled-CoFe$_2$O$_4$ ferrite exhibited excellent electrochemical performance, governed by mass transport over an electroactive area of 0.0046 cm^2. The resulting electrochemical sensor showed good performance, with exhibited a coefficient of determination of 0.9987, a sensitivity of 3.352 ± 0.0428 μA mol L^{-1}, and a limit of detection of 0.5511 μM in the concentration range of 1.96 to 23.08 mmol L^{-1} for AA detection. This study demonstrated that sufficiently pure CoFe$_2$O$_4$ nanoparticles can be prepared from battery waste and mine tailings and supplemented with other inputs for enhanced value and application in environmentally friendly reactions.

Supplementary Information

Supplementary information (schematic of the complete experimental procedure, complementary illustrations explaining the decolorization of MB dye, and other analysis) is available free of charge at http://jbcs.sbq.org.br as PDF file.

Acknowledgments

Author Contributions

Jenifer R. Almeida was responsible for conceptualization, data curation, formal analysis, investigation, methodology, visualization, original draft writing, review and editing; Mayra N. Moura, Luma B. Magnago and Ana K. S. Rocha for data curation, investigation, methodology, visualization, writing the original draft, review and editing; Edson L. D. Carvalho for part of the methodology; Sandra A. D. Ferreira, Maria F. F. Lelis and Marcos B. J. G. de Freitas for the conceptualization, investigation, methodology, resources, supervision, project administration, obtaining financing, visualization, writing the original draft, reviewing and editing.

References

1. Ádám, B.; Göen, T.; Scheepers, P. T. J.; Adliene, D.; Batinic, B.; Budnik, L. T.; Duca, R. C.; Ghosh, M.; Giurgiu, D. I.; Godderis, L.; Goksel, O.; Hansen, K. K.; Kassomenos, P.; Milic, N.; Orru, H.; Paschalidou, A.; Petrovic, M.; Puiso, J.; Radonic, J.; Sekulic, M. T.; Teixeira, J. P.; Zaid, H.; Au, W. W.; *Environ. Res.* **2021**, *194*, 110728. [Crossref] [PubMed]

2. Jain, M.; Kumar, D.; Chaudhary, J.; Kumar, S.; Sharma, S.; Singh Verma, A.; *Waste Manage. Bull.* **2023**, *1*, 34. [Crossref]

3. Statista Research Department; *Electronic Waste Generation Worldwide in 2022, with a Projection for 2030*, https://www.statista.com/statistics/1067081/generation-electronic-waste-globally-forecast/, accessed in July 2024.

4. Park, Y. K.; Song, H.; Kim, M. K.; Jung, S.-C.; Jung, H. Y.; Kim, S. C.; *J. Hazard. Mater.* **2021**, *403*, 123929. [Crossref]

5. Resíduos Eletrônicos no Brasil, https://greeneletron.org.br/pesquisa-2023, accessed in July 2024.

6. Shahjalal, M.; Roy, P. K.; Shams, T.; Fly, A.; Chowdhury, J. I.; Ahmed, M. R.; Liu, K.; *Energy* **2022**, *241*, 122881. [Crossref]

7. How to Get Better MFI Results; https://www.ptonline.com/articles/how-to-get-better-mfi-results, accessed in July 2024.

8. Qu, G.; Li, B.; Wei, Y.; *Chem. Eng. J.* **2023**, *451*, 138897. [Crossref]

9. Ahirwar, R.; Tripathi, A. K.; *Environ. Nanotechnol., Monit. Manage.* **2021**, *15*, 100409. [Crossref]

10. Leal, V. M.; Ribeiro, J. S.; Coelho, E. L. D.; Freitas, M. B. J. G.; *J. Energy Chem.* **2023**, *79*, 118. [Crossref]

11. Almeida, J. R.; Moura, M. N.; Barrada, R. V.; Barbieri, E. M. S.; Carneiro, M. T. W. D.; Ferreira, S. A. D.; Lelis, M. F. F.; de Freitas, M. B. J. G.; Brandão, G. P.; *Sci. Total Environ.* **2019**, *685*, 589. [Crossref]

12. Jing, Q.; Zhang, J.; Liu, Y.; Zhang, W.; Chen, Y.; Wang, C.; *ACS Sustainable Chem. Eng.* **2020**, *8*, 17622. [Crossref]

13. Fei, Z.; Zhou, S.; Zhang, Y.; Meng, Q.; Dong, P.; Li, Y.; Fei, J.; Qi, H.; Yan, J.; Zhao, X.; *ACS Sustainable Chem. Eng.* **2022**, *10*, 6853. [Crossref]

J. Braz. Chem. Soc. **2025**, *36*, 2, e-20240137

15 of 17

14. Zhou, S.; Zhang, Y.; Meng, Q.; Dong, P.; Fei, Z.; Li, Q.; *J. Environ. Manage.* **2021**, *277*, 111426. [Crossref] [PubMed]

15. Gueye, R. S.; Gaye, N.; Baldé, M.; Diedhiou, A.; Diouf, N.; Awa, S. G.; Ndoye, I.; Tine, Y.; Seck, M.; Fall, D.; Wele, A.; Diaw, M.; *Open J. Inorg. Chem.* **2022**, *12*, 19. [Crossref]

16. Fundação Estadual do Meio Ambiente (FEAM); *Inventário de Barragem do Estado de Minas Gerais Ano Base 2017*; FEAM: Belo Horizonte, 2018. [Link] accessed in July 2024

17. Marta-Almeida, M.; Mendes, R.; Amorim, F. N.; Cirano, M.; Dias, J. M.; *Mar. Pollut. Bull.* **2016**, *112*, 359. [Crossref] [PubMed]

18. Carmignano, O. R.; Vieira, S. S.; Teixeira, A. P. C.; Lameiras, F. S.; Brandão, P. R. G.; Lago, R. M.; *J. Braz. Chem. Soc.* **2021**, *32*, 1895. [Crossref]

19. Figueiredo, M. D.; Lameiras, F. S.; Ardisson, J. D.; Araujo, M. H.; Teixeira, A. P. C.; *Integr. Environ. Assess. Manage.* **2019**, *16*, 636. [Crossref]

20. Almeida, C. A.; de Oliveira, A. F.; de Pacheco, A. A.; Lopes, R. P.; Neves, A. A.; de Queiroz, M. E. L. R.; *Chemosphere* **2018**, *209*, 411. [Crossref] [PubMed]

21. Mossali, E.; Picone, N.; Gentilini, L.; Rodrìguez, O.; Pérez, J. M.; Colledani, M.; *J. Environ. Manage.* **2020**, *264*, 110500. [Crossref] [PubMed]

22. Zhan, L.; Jiang, L.; Zhang, Y.; Gao, B.; Xu, Z.; *Chem. Eng. J.* **2020**, *390*, 124651. [Crossref]

23. Magnago, L. B.; Betim, F. S.; Almeida, J. R.; Moura, M. N.; Coelho, E. L. D.; Leal, V. M.; Ferreira, S. A. D.; Lelis, M. F. F.; Freitas, M. B. J. G.; *J. Braz. Chem. Soc.* **2024**, *35*, e-20230184. [Crossref]

24. Thejas, H. K.; Hossiney, N.; *Case Stud. Constr. Mater.* **2022**, *16*, e00973. [Crossref]

25. de Freitas, V. A. A.; Breder, S. M.; Silvas, F. P. C.; Rouse, P. R.; de Oliveira, L. C. A.; *Chemosphere* **2019**, *219*, 328. [Crossref] [PubMed]

26. Behura, R.; Sakthivel, R.; Das, N.; *Powder Technol.* **2021**, *386*, 519. [Crossref]

27. Lelis, M. F. F.; Porto, A. O.; Gonçalves, C. M.; Fabris, J. D.; *J. Magn. Magn. Mater.* **2004**, *278*, 263. [Crossref]

28. Soufi, A.; Hajjaoui, H.; Elmoubarki, R.; Abdennouri, M.; Qourzal, S.; Barka, N.; *Appl. Surf. Sci. Adv.* **2021**, *6*, 100145. [Crossref]

29. Chaibakhsh, N.; Moradi-Shoeili, Z.; *Mater. Sci. Eng., C* **2019**, *99*, 1424. [Crossref]

30. Oladipo, A. A.; Gazi, M.; *React. Funct. Polym.* **2016**, *109*, 23. [Crossref]

31. Jung, K. W.; Lee, S.; Lee, Y. J.; *Bioresour. Technol.* **2017**, *245*, 751. [Crossref] [PubMed]

32. Shah, J.; Kotnala, R. K.; *Sens. Actuators, B* **2012**, *171*, 832. [Crossref]

33. Zafar, Q.; Azmer, M. I.; Al-Sehemi, A. G.; Al-Assiri, M. S.; Kalam, A.; Sulaiman, K.; *J. Nanoparticle Res.* **2016**, *18*, 186. [Crossref]

34. Zhang, J.; Zhang, C.; Li, Y.; Xiao, J.; Zhang, Y.; Jia, M.; Lu, L.; Zhang, H.; Zhou, J.; Zhang, Z.; Du, X.; *Chem. Eng. J.* **2023**, *471*, 144797. [Crossref]

35. Amiri, S.; Shokrollahi, H.; *Mater. Sci. Eng., C* **2013**, *33*, 1. [Crossref] [PubMed]

36. Mathew, D. S.; Juang, R. S.; *Chem. Eng. J.* **2007**, *129*, 51. [Crossref]

37. Proveti, J. R. C.; Porto, P. S. S.; Muniz, E. P.; Pereira, R. D.; Araujo, D. R.; Silveira, M. B.; *J. Sol-Gel Sci. Technol.* **2015**, *75*, 31. [Crossref]

38. Žalnėravičius, R.; Paškevičius, A.; Kurtinaitiene, M.; Jagminas, A.; *J. Nanopart. Res.* **2016**, *18*, 300. [Crossref]

39. Yan, F.; Shi, Y.; Zhou, X.; Zhu, K.; Shen, B.; Zhai, J.; *Chem. Eng. J.* **2021**, *417*, 127945. [Crossref]

40. Meng, F.; Liu, Q.; Kim, R.; Wang, J.; Liu, G.; Ghahreman, A.; *Hydrometallurgy* **2020**, *191*, 105160. [Crossref]

41. Pi, Y.; Gao, H.; Cao, Y.; Cao, R.; Wang, Y.; Sun, J.; *Chem. Eng. J.* **2020**, *379*, 122377. [Crossref]

42. Zhou, Y.; Xiao, B.; Liu, S.-Q.; Meng, Z.; Chen, Z.-G.; Zou, C.-Y.; Liu, C.-B.; Chen, F.; Zhou, X.; *Chem. Eng. J.* **2016**, *283*, 266. [Crossref]

43. Biazati, L. B.; Moreira, T. F. M.; Neto, R. R.; Teixeira, A. L.; Freitas, M. B. J. G.; Lelis, M. F. F.; *Rev. Virtual Quim.* **2017**, *9*, 848. [Crossref]

44. Ferreira, S. A. D.; Donadia, J. F.; Gonçalves, G. R.; Teixeira, A. L.; Freitas, M. B. J. G.; Fernandes, A. A. R.; Lelis, M. F. F.; *J. Environ. Chem. Eng.* **2019**, *7*, 103144. [Crossref]

45. Rocha, A. K. S.; Magnago, L. B.; Santos, J. J.; Leal, V. M.; Marins, A. A. L.; Pegoretti, V. C. B.; Ferreira, S. A. D.; Lelis, M. F. F.; Freitas, M. B. J. G.; *Mater. Res. Bull.* **2019**, *113*, 231. [Crossref]

46. Magnago, L. B.; Rocha, A. K. S.; Pegoretti, V. C. B.; Ferreira, S. A. D.; Lelis, M. F. F.; Freitas, M. B. J. G.; *Ionics* **2019**, *25*, 2361. [Crossref]

47. Morais, V. S.; Barrada, R. V.; Moura, M. N.; Almeida, J. R.; Moreira, T. F. M.; Gonçalves, G. R.; Ferreira, S. A. D.; Lelis, M. F. F.; Freitas, M. B. J. G.; *J. Environ. Chem. Eng.* **2020**, *8*, 103716. [Crossref]

48. Moura, M. N.; Barrada, R. V.; Almeida, J. R.; Moreira, T. F. M.; Schettino, M. A.; Freitas, J. C. C.; Ferreira, S. A. D.; Lelis, M. F. F.; Freitas, M. B. J. G.; *Chemosphere* **2017**, *182*, 339. [Crossref]

49. Ribeiro, J. S.; Moreira, T. F. M.; Santana, I. L.; Ferreira, S. A. D.; Lelis, M. F. F.; Freitas, M. B. J. G.; *Mater. Chem. Phys.* **2018**, *205*, 186. [Crossref]

50. Wang, Z.; You, J.; Li, J.; Xu, J.; Li, X.; Zhang, H.; *Catal. Sci. Technol.* **2023**, *13*, 274. [Crossref]

51. Wang, J.; Wang, S.; *Chem. Eng. J.* **2020**, *401*, 126158. [Crossref]

52. Irani, M.; Roshanfekr, L.; Pourahmad, H.; Haririan, I.; *Microporous Mesoporous Mater.* **2015**, *206*, 1. [Crossref]

53. Qiu, B.; Deng, Y.; Du, M.; Xing, M.; Zhang, J.; *Sci. Rep.* **2016**, *6*, 29099. [Crossref]

54. Vinosha, P. A.; Das, S. J.; *Mater. Today: Proc.* **2018**, *5*, 8662. [Crossref]

55. Kalam, A.; Al-Sehemi, A. G.; Assiri, M.; Du, G.; Ahmad, T.; Ahmad, I.; Pannipara, M.; *Results Phys.* **2018**, *8*, 1046. [Crossref]

56. Hoang, V. T.; Trang, N. L. N.; Nga, D. T. N.; Ngo, X. D.; Pham, T. N.; Tran, V. T.; Mai, M.; Tam, L. T.; Tri, D. Q.; Le, A. T.; *Adv. Nat. Sci.: Nanotechnol.* **2022**, *13*, 035002. [Crossref]

57. Charan, C.; Shahi, V. K.; *RSC Adv.* **2016**, *6*, 59457. [Crossref]

58. Avan, A. A.; Filik, H.; *Curr. Nanosci.* **2018**, *14*, 199. [Crossref]

59. Asadpour-Zeynali, K.; Lotfi, N.; *Micro Nano Lett.* **2019**, *14*, 1397. [Crossref]

60. Katowah, D. F.; Rahman, M. M.; Hussein, M. A.; Sobahi, T. R.; Gabal, M. A.; Alam, M. M.; Asiri, A. M.; *Composites, Part B* **2019**, *175*, 107175. [Crossref]

61. Banavath, R.; Abhinav, A.; Srivastava, R.; Bhargava, P.; *Electrochim. Acta* **2022**, *419*, 140335. [Crossref]

62. Leal, V. M.; Magnago, L. B.; dos Santos, G. F. S.; Ferreira, R. Q.; Ferreira, S. A. D.; Lelis, M. F. F.; Freitas, M. B. J. G.; *Sustainable Mater. Technol.* **2023**, *37*, e00688. [Crossref]

63. Barbieri, E. M. S.; Lima, E. P. C.; Cantarino, S. J.; Lelis, M. F. F.; Freitas, M. B. J. G.; *J. Power Sources* **2014**, *269*, 158. [Crossref]

64. ABNT NBR 10007:2004: *Amostragem de Resíduos Sólidos*, Associação Brasileira de Normas Técnicas (ABNT), Rio de Janeiro, 2004. [Link] accessed in July 2024

65. Teixeira, P. C.; Donagemma, G. K.; Fontana, A.; Teixeira, W. G.; *Manual de Métodos de Análise de Solo*; Embrapa: Brasília, 2017. [Link] accessed in July 2024

66. ABNT NBR 7181:2016: *Solo - Análise Granulométrica*, Associação Brasileira de Normas Técnicas (ABNT), Rio de Janeiro, 2016. [Link] accessed in July 2024

67. Shirsath, S. E.; Wang, D.; Jadhav, S. S.; Mane, M. L.; Li, S.; *Handbook of Sol-Gel Science and Technology*: Springer International Publishing: Cham, 2018. [Crossref]

68. Venturini, J.; Zampiva, R. Y. S.; Arcaro, S.; Bergmann, C. P.; *Ceram. Int.* **2018**, *44*, 12381. [Crossref]

69. Centro de Referência para as Energias Solar e Eólica Sérgio de S. Brito, http://www.cresesb.cepel.br/index.php#data accessed in July 2024.

70. Pegoretti, V. C. B.; Dixini, P. V. M.; Magnago, L.; Rocha, A. K. S.; Lelis, M. F. F.; Freitas, M. B. J. G.; *Mater. Res. Bull.* **2019**, *110*, 97. [Crossref]

71. Scherrer, P.; *Gott. Nachr Math. Phys* **1918**, *2*, 98.

72. Bessy, T. C.; Bindhu, M. R.; Johnson, J.; Rajagopal, R.; Kuppusamy, P.; *Chemosphere* **2022**, *299*, 134396. [Crossref] [PubMed]

73. Yang, L.; Xi, G.; Lou, T.; Wang, X.; Wang, J.; He, Y.; *Ceram. Int.* **2016**, *42*, 1897. [Crossref]

74. Wen, C.; Zhu, Y. J.; Kanbara, T.; Zhu, H. Z.; Xiao, C. F.; *Desalination* **2009**, *249*, 621. [Crossref]

75. Li, Y.; Liu, Y.; Liu, Y.; Chen, Y.; Chen, L.; Yan, H.; Chen, Y.; Xu, F.; Li, M.; Li, L.; *J. Water Process Eng.* **2022**, *48*, 102864. [Crossref]

76. Teng, X.; Li, J.; Wang, Z.; Wei, Z.; Chen, C.; Du, K.; Zhao, C.; Yang, G.; Li, Y.; *RSC Adv.* **2020**, *10*, 24712. [Crossref]

77. Uzunoğlu, D.; Ergüt, M.; Karacabey, P.; Özer, A.; *Desalin. Water Treat.* **2019**, *172*, 96. [Crossref]

78. Casbeer, E.; Sharma, V. K.; Li, X.-Z.; *Sep. Purif. Technol.* **2012**, *87*, 1. [Crossref]

79. Araujo, F. V. F.; Yokoyama, L.; Teixeira, L. A. C.; *Quim. Nova* **2006**, *29*, 11. [Crossref]

80. Han, X.; Zhao, Y.; Zhao, F.; Wang, F.; Tian, G.; Liang, J.; *Colloids Surf., A* **2023**, *656*, 130412. [Crossref]

81. Nadeem, N.; Yaseen, M.; Rehan, Z. A.; Zahid, M.; Shakoor, R. A.; Jilani, A.; Iqbal, J.; Rasul, S.; Shahid, I.; *Environ. Res.* **2022**, *206*, 112280. [Crossref]

82. Gnaser, H.; Savina, M. R.; Calaway, W. F.; Tripa, C. E.; Veryovkin, I. V.; Pellin, M. J.; *Int. J. Mass Spectrom.* **2005**, *245*, 61. [Crossref]

83. Conselho Nacional do Meio Ambiente (CONAMA); https://conama.mma.gov.br/images/conteudo/LivroConama.pdf, accessed in July 2024.

84. Ferreira, L. S.; Silva, T. R.; Silva, V. D.; Simões, T. A.; Araújo, A. J. M.; Morales, M. A.; Macedo, D. A.; *Adv. Powder Technol.* **2020**, *31*, 604. [Crossref]

85. Pakapongpan, S.; Mensing, J. P.; Phokharatkul, D.; Lomas, T.; Tuantranont, A.; *Electrochim. Acta* **2014**, *133*, 294. [Crossref]

86. Thu, P. T. K.; Trinh, N. D.; Hoan, N. T. V.; Du, D. X.; Mau, T. X.; Trung, V. H.; Phong, N. H.; Toan, T. T. T.; Khieu, D. Q.; *J. Mater. Sci. Mater. Electron.* **2019**, *30*, 17245. [Crossref]

J. Braz. Chem. Soc. **2025**, *36*, 2, e-20240137

17 of 17